NIH Public Access
Author Manuscript
J Phys Chem A. Author manuscript; available in PMC 2013 July 30.

Published in final edited form as:
J Phys Chem A. 2008 February 14; 112(6): 1286–1293. doi:10.1021/jp0763937.

On the Dynamics of Fragment Isomerization in Collision-Induced Dissociation of Peptides

Nick C. Polfer[*,†], **Brian C. Bohrer**[‡], **Manolo D. Plasencia**[‡], **Béla Paizs**[§], and **David E. Clemmer**[‡]
Department of Chemistry, University of Florida, Gainesville, Florida 32611, Department of Chemistry, Indiana University, Bloomington, Indiana 47405, and German Research Center, Im Neuenheimer Feld 580, D-69120 Heidelberg, Germany

Abstract

The structures of peptide collision-induced dissociation (CID) product ions are investigated using ion mobility/ mass spectrometry techniques combined with theoretical methods. The cross-section results are consistent with a mixture of linear and cyclic structures for both $\mathbf{b_4}$ and $\mathbf{a_4}$ fragment ions. Direct evidence for cyclic structures is essential in rationalizing the appearance of fragments with scrambled (*i.e.,* permutated) primary structures, as the cycle may not open up where it was initially formed. It is demonstrated here that cyclic and linear $\mathbf{a_4}$ structures can interconvert freely as a result of collisional activation, implying that isomerization takes place prior to dissociation.

Introduction

Although it is generally understood that the amino acid chains that comprise peptides in solution are highly dynamic, one does not expect a change in the primary structure (*i.e.*, amino acid sequence) of these molecules to occur. However, in the gas phase, where it is possible to add substantial internal energy, the fragments of these linear structures can undergo rearrangement processes in which the sequence appears to change.[1,2] This is especially true when peptide ions are subjected to collisions with a background gas to induce collision-induced dissociation (CID). Generally, the masses of the CID product ions are expected to reflect the amino acid sequence of the peptide and therefore be valuable for sequencing.[3,4] In fact, this approach is now a cornerstone in the identification of proteins by mass spectrometry.[5,6] The interpretation of these spectra is often carried out using computer algorithms.[7,8] With current methods a large fraction of examined ions cannot be identified.[9] At least in part, this is due to an incomplete understanding of the underlying fragmentation chemistry.[10]

As background, it is well-known that under CID conditions, protonated peptide ions generally display abundant cleavages at the backbone amide bonds, giving rise to N-terminal **b** and C-terminal **y** product ions.[11] In proposed mechanisms, the ionizing proton is thought to be moved from a site of higher proton affinity, such as a basic side chain (*e.g.,* guanidine group of arginine), to the backbone C=O and then NH groups, thereby weakening the amide bond.[12,13] Although there has been controversy about the dissociation mechanism and the

© 2008 American Chemical Society

[*]Corresponding author. polfer@chem.ufl.edu.
[†]University of Florida.
[‡]Indiana University.
[§]German Research Center.

Supporting Information Available: Reaction scheme (Scheme S1), ion mobility spectra (Figure S2), mobility selections (S3) and activations (S4). This information is available free of charge via the Internet at http://pubs.acs.org.

NIH-PA Author Manuscript
NIH-PA Author Manuscript
NIH-PA Author Manuscript

NIH-PA Author Manuscript

NIH-PA Author Manuscript

NIH-PA Author Manuscript

types of structures that are formed (especially for **b** fragment ions),[14–18] it is now generally accepted that the most likely dissociation pathway occurs via nucleophilic attack from a backbone carbonyl oxygen to a carbonyl carbon, thus forming a five-membered "oxazolone" ring **b** fragment structure.[16,18] This is exemplified in the reaction chemistry of the pentapeptide Leu-enkephalin (Tyr-Gly-Gly-Phe-Leu) that we have chosen in this study (see Scheme 1A, B). Detailed *ab inito* calculations have confirmed that this pathway is both energetically and entropically accessible.[10] Moreover, the presence of oxazolone-type structures has recently been corroborated on the basis of structurally diagnostic oxazolone C=O stretch modes by infrared (IR) spectroscopy.[19,20] Linear oxazolone structures are believed to be able to isomerize to fully cyclic structures, following a nucleophilic attack by the N-terminus on the oxazolone ring (Scheme 1C).[2] If the cyclic structure opens up at a different amide bond than where it was originally formed, this results in oxazolone structures with permutated (*i.e.*, scrambled) primary structures (gray box, Scheme 1D). The subsequent CID of these scrambled structures is responsible for the appearance of "nondirect" CID fragments,[2] which cannot be explained on the basis of the original amino acid sequence of the peptide.

Experimental evidence for such cyclic structures comes from IR spectroscopy; however, the assignment is less definite than in the case of oxazolone structures, and it is difficult to draw conclusions on the relative abundances of the different isomers in the mixture.[20] Other indicative evidence for cyclic structures comes from H/D exchange studies[21] and ion mobility measurements.[22] It should be noted that cyclic configurations are not limited to **b** ions but can also occur for other N-terminal fragments, such as for instance **a** fragments (*i.e.*, the **b** ion less a CO). In analogy to $\mathbf{b_4}$, Leu-enkephalin $\mathbf{a_4}$ is thought to adopt both linear imine (E) and cyclic structures (F) (Scheme 1).[20] A re-opening of the cyclic isomers can again give rise to permutated oxazolone-type structures (gray box G), the subsequent CID of which rationalizes nondirect sequence ions.

Here, we present a systematic study of the structural products that are formed in collision-induced dissociation of the pentapeptide Leu-enkephalin by ion mobility/mass spectrometry.[23,24] These products are also compared to the fragments for *N*-acetyl Leu-enkephalin. We address the question of the relative abundances of the different structural isomers, and whether the relative abundances can be influenced by the amount of energy deposited in the molecule. This result provides insights into the dynamics of the isomerization pathways, which are important in peptide scrambling processes. This is also the first study that uses ion mobility in combination with theoretical approaches to answer structural questions on CID fragment ions.

Methods

Ion Mobility/Mass Spectrometry Measurements

The protonated pentapeptide Leu-enkephalin (Tyr-Gly-Gly-Phe-Leu) (Sigma Aldrich, St. Louis) precursor ion was generated by electrospray ionization (ESI).[25] The ions were trapped in an rf ion funnel prior to pulsed extraction into an intermediate pressure He-filled drift tube (~3 Torr). Ions travel the length of the drift tube under the influence of an electric field (~9 V cm^{-1}) but are retarded in their motion due to collisions with the He background gas. Ions of different collision cross-sections are thus separated in space and will arrive at the detector at different times, defined as the drift time or arrival time distributions.

The laboratory-constructed drift tube design employed in these experiments has been described in detail previously.[26] Briefly, it is made up of three consecutive drift tubes, each 0.9 m in length, and the series is followed by an orthogonal time-of-flight mass analyer. At the end of each drift tube, the radially diffuse ion population is re-focused using an rf ion

NIH-PA Author Manuscript

NIH-PA Author Manuscript

NIH-PA Author Manuscript

funnel, which is operated at the same pressure as the drift tube. This improves the overall transmission of ions through the drift tube.[27] Moreover, by selecting ions of a specific mobility at the end of the first drift tube it is possible to select specific conformers, re-focus these selected ions in the ion funnel, and collisionally activate the mobility-selected ions for injection into the second drift tube.[28,29] Additional mobility selections and activations can be carried out in each consecutive drift tube, thus allowing a multistage IMS approach,[28] in analogy to multiple mass isolations (MS/MS).

Experimental Cross-Sections

Singly protonated Leu-en-kephalin (m/z 556) was determined to have an experimentally derived collision cross-section Ω ~162 Å^2, based on the drift time in the first drift tube. The procedure to calculate cross-sections has been described in detail many times before[23,24] and is based on the relation

$$\Omega=\frac{(18\pi)^{1/2}}{16}\frac{ze}{(k_BT)^{1/2}}\left[\frac{1}{m_I}+\frac{1}{m_B}\right]^{1/2}\frac{t_DE}{L}\frac{760}{P}\frac{T}{273.2}\frac{1}{N} \quad (1)$$

where z, e, k_B, m_I and m_B, and N denote fundamental properties such as the charge state, elemental charge, Boltzmann's constant, mass of the ion and mass of the buffer gas, and the neutral number density, respectively. The experimental parameters E, L, P, T and t_D correspond to the applied electric field, length of the drift tube (m), pressure (Torr), temperature (K) and arrival time (s).

Under the experimental conditions used, the precursor Leu-enkephalin ion was efficiently mobility-selected by using a 100 μs-wide voltage gating window at the end of the first drift tube (after ~11.8 ms drift time). This precursor ion was then activated by applying a voltage drop between two adjacent rings (up to 230 V over a 3 mm spacing) at the end of the ion funnel,[26] thus generating a number of CID product ions, of which $\mathbf{y_4}$ (m/z 393), $\mathbf{a_4}$ (m/z 397) and $\mathbf{b_4}$ (m/z 425) were among the most abundant. The experimental collision cross-sections of the Leu-enkephalin $\mathbf{a_4}$ and $\mathbf{b_4}$ ions were calculated from the drift time distributions in the second drift tube. This drift time could be accurately determined on the basis of the mobility selection of the precursor Leu-enkephalin at the end of the first drift tube, the known mobility of the precursor up to the activation region at the end of the ion funnel and the mobility selections of the CID fragments at the end of the second drift tube. The "unknown quantity" in this approximation is the temporary change in mobility due to collisional activation and the unknown time for complete thermalization. Nonetheless, the decrease in the drift time of the precursor ion due to collisional activation could be accurately determined and this serves as a good estimate for the "unknown quantity" above. It was found that this decrease in drift time was on the order of 100–200 μs for drift times of ~10 ms through 1 drift tube. This decrease in drift time was taken into account when calculating the cross-sections, thus bringing the total error of the measurement in the range of 1–2%, as commonly expected in ion mobility measurements.[30,31] The CID product ion drift time distributions of Leu-enkephalin were also compared to those for N-acetylated Leu-enkephalin. The latter peptide was made by using acetic anhydride to couple an acetyl group to the N-terminus.

Calculations

A detailed theoretical investigation of the fragment structures for $\mathbf{b_4}$ and $\mathbf{a_4}$ of Leu-enkephalin has been published before,[20] and the density-functional theory geometries (B3LYP/6-31+G(d,p)) and atomic charges of the optimized structures were used to calculate theoretical cross-sections. We used the trajectory method in the MOBCAL program

NIH-PA Author Manuscript

NIH-PA Author Manuscript

NIH-PA Author Manuscript

developed by the Jarrold group, which includes He-ion long-range interactions.[32] In the nomenclature of the $\mathbf{a_4}$ imine structures, the same notation was used as in the previous publication.[20] "IM TR N-term-prot" refers the trans imine structure that is protonated on the N-terminus. "IM CI imine-prot" denotes the cis imine structure that is protonated on the imine nitrogen. "Cyc N-prot" refers to the fully cyclic structure of $\mathbf{a_4}$, which is protonated on the nitrogen that was previously included in the imine group. The chemical structures are also displayed in Scheme 1.

Results and Discussion

Comparison of Leu-Enkephalin and *N*-Acetyl Leu-En-kephalin

Protonated Leu-enkephalin (m/z 556) and *N*-acetyl Leu-enkephalin (m/z 598) were mobility-selected in the same experiment and subjected to collision-induced dissociation under identical conditions, giving rise to their respective $\mathbf{b_4}$ (m/z 425 and 467) and $\mathbf{a_4}$ (m/z 397 and 439) fragments. The total drift time distributions of each of these fragments are presented in Figure 1; note that the total drift time corresponds to the sum of the drift times that the ions spend in different parts of the split drift tube design. The longer drift times for the N-acetylated Leu-enkephalin fragments, relative to the Leu-enkephalin fragments, are not surprising, given the bulky acetyl group. However, the differences between the **b** and **a** arrival time distributions are much more telling. The $\mathbf{b_4}$ fragments of Leu-enkephalin (Figure 1C) and *N*-acetyl Leu-enkephalin (Figure 1D) display relatively narrow peaks, whereas the distributions for $\mathbf{a_4}$ are much broader, and clearly involve multiple structures. The drift time distribution of other CID products, such as $\mathbf{y_4}$ (Figure S2), also only show one main feature. It is interesting to note that the drift time distribution of Leu-enkephalin $\mathbf{a_4}$ in Figure 1 has at least three identifiable peaks (centered at ~31.6, 32.2 and 33.45 ms) but *N*-acetyl Leu-enkephalin $\mathbf{a_4}$ just exhibits two main features (centered at 34.6 and 35 ms). Admittedly, the third peak at 33.45 ms is of low intensity, but it was reproduced independently on multiple measurements (see also Figure S2, Supporting Information). Other studies have also shown that multiple CID product ion structures can be resolved by ion mobility,[22,28] though no theoretical analysis was done in those studies. Our assignment of the mobility-separated structures in Figure 1 is tentatively indicated, and each of these will be discussed in detail in the following section.

The dissociation chemistry of Leu-enkephalin and N-acetylated Leu-enkephalin is expected to be quite different: due to the presence of the *N*-acetyl group, fragments of N-acetylated Leu-enkephalin cannot adopt a fully cyclic structure (see Scheme S1, Supporting Information). Moreover, proton attachment on the N-terminus is no longer possible, thus making the imine N unambiguously the most basic site in the **a**-ion structure. This limits the number of putative structures that have to be considered to the cis and trans imine configurations. It is thus tempting to assign the two mobility-separated peaks as cis and trans imine, as we have done in Figure 1B. It is worth noting, however, that the trans form is energetically more favored than the cis one.[20] The above assignment clearly contradicts this energetics, because it suggests that the cis form is more favored than the trans structure. Further theoretical investigations are underway in our laboratories to resolve this controversy. Preliminary molecular mechanics modeling suggest that there is no significant difference in the predicted collision cross-sections between cis and trans imine structures (not shown).

Leu-Enkephalin $\mathbf{a_4}$

Figure 2B shows the mobility distribution of Leu-enkephalin $\mathbf{a_4}$ on a collision cross-section scale. This mobility distribution was derived from the experimental drift time distribution of $\mathbf{a_4}$ (Figure S3) and mobility selections (1–3) at the end of the second drift tube. The

NIH-PA Author Manuscript

NIH-PA Author Manuscript

NIH-PA Author Manuscript

corresponding cross-section for each selection was determined from the drift time through the second drift tube (as described in the Methods), thus allowing a conversion of the total drift time distribution into a cross-section scale. The mobility selections are displayed in Figure 2B and the experimental features are labeled as I, II and III for the sake of the discussion hereafter.

For Leu-enkephalin $\mathbf{a_4}$ many more structural possibilities have to be considered compared to the N-acetylated variant, including imine structures with proton attachment to the N-terminus, the cyclic conformer, as well as oxazolone-type $\mathbf{a_4}$ structures (see Scheme 1 and nomenclature in the Methods). A detailed study of many of these conformers has already been presented,[20] and we make use of the lowest-energy structures from that study to try to explain the results shown here. The theoretical cross-sections of the four lowest-energy conformers of each imine variant are presented in Figure 2A, as well as the six lowest-energy conformers of the cyclic structure. The average theoretical collision cross-sections and the standard deviations for each structural variant of $\mathbf{a_4}$ are also summarized in Table 1. On the basis of the IR spectroscopy study,[20] N-terminal-protonated imine and cyclic structures could be confirmed, whereas imine-protonated and oxazolone-type $\mathbf{a_4}$ were excluded. Note that the latter oxazolone-type $\mathbf{a_4}$ structures were not excluded on the basis of the calculated structures, but rather on the absence of an oxazolone CO stretch in the IR spectrum for $\mathbf{a_4}$.[20]

A comparison of the calculated cross-sections to the experimental results shows that the most compact structure (I) could be explained by the cyclic geometry (orange pentagons), whereas the most extended conformer (III) matches the trans imine N-terminal-protonated structure (red triangles).[26] Feature II could be rationalized by the cis imine N-terminal protonated structures (blue dots). It is nonetheless odd that the higher-energy cis imine should be much more abundant than trans imine, the relative contributions of the different structures being estimated at 31% I, 61% II and 8% III. We are currently performing further calculations to resolve this contradiction.

The theoretical approach followed here involves generating zero-energy structures and corresponding predicted collision cross-sections, which are then compared to experimentally determined cross-sections. This is probably not an accurate reflection of the dynamic structures that are actually probed by ion mobility. As one compares the theoretical mobilities of the lower- to the higher-energy imine structures, one observes a general decrease in the calculated cross-sections (*i.e.*, increase in mobility). This is contrary to what one may expect intuitively, but it suggests that the 300 K mobilites may actually be higher than what is predicted for the lowest-energy zero-K structures. The cyclic configurations, on the other hand, have consistently high mobilities. This is in fact expected from their compact structures and constrained flexibility compared to linear structures. The large range in predicted cross-sections for the linear imine structures is probably due to the combination of a highly flexible backbone around the glycine residues and the presence of bulky aromatic side chains (Phe and Tyr) near the termini, which make an accurate prediction of the collision cross-section challenging. In summary, the structural assignment of the most compact $\mathbf{a_4}$ ions as cyclic structures and the most extended structures as linear trans imine structures is relatively convincing; however, the interpretation of feature II remains to be clarified.

Leu-Enkephalin $\mathbf{b_4}$

The mobility distribution of Leu-enkephalin $\mathbf{b_4}$ on a cross-section scale is shown in Figure 3B. The procedure to derive cross-section distributions from drift time distributions is again the same as for $\mathbf{a_4}$. The predicted cross-sections and relative energies of five oxazolone and three cyclic structures are displayed in Figure 3A and their average cross-sections are

NIH-PA Author Manuscript

NIH-PA Author Manuscript

NIH-PA Author Manuscript

summarized in Table 1. The experimentally derived cross-sections agree well with the predicted cross-sections for the cyclic structure but give an inadequate match to the lowest-energy oxazolone-type structures. This is surprising, as oxazolone structures have been identified by IR spectroscopy for this particular $\mathbf{b_4}$ fragment.[19,20] Under the CID conditions here, similar fragment structures would be expected to be observed as in that previous study. The higher-energy calculated oxazolone conformers exhibit increased mobility, in analogy to the higher-energy imine $\mathbf{a_4}$ conformers, thus at least approaching the experimentally determined cross-sections. In conclusion, it is highly probable that oxazolone structures are formed in the case of $\mathbf{b_4}$, which also suggests that the theoretical cross-sections from zero-energy structures consistently overestimate the actual cross-sections of the linear fragments at room temperature.

An argument in favor of a mixture of oxazolone and cyclic structures for $\mathbf{b_4}$ can be made in light of the broader peak in the drift time distributions for Leu-enkephalin $\mathbf{b_4}$ (Figure 1C) compared to *N*-acetyl Leu-enkephalin $\mathbf{b_4}$ (Figure 1D) under identical experimental conditions. The broader peak shape of Leu-enkephalin $\mathbf{b_4}$ is consistent with a mixture of structures, in contrast to *N*-acetyl Leu-enkephalin $\mathbf{b_4}$, where the cyclic structure cannot be formed. It is also interesting that the weak feature at 127 $Å^2$ is consistently reproduced, although a structural assignment could not be made yet.

CID Activation Energy

To assess the influence of the energy deposited in the CID process on the relative abundances of the CID product ions, the activation energy was varied from 180 to 220 V, as shown in Figure 4A, B. At the lower activation energy, the fragmentation yield is low and $\mathbf{b_4}$ dominates, whereas at the higher activation energy other products ($\mathbf{b_3}$, $\mathbf{y_3}$, $\mathbf{y_4}$ and $\mathbf{a_4}$) become competitive. This has in fact been shown in other studies[2,33] and does therefore not come as a surprise. On the other hand, if one compares the drift time distributions of $\mathbf{a_4}$ as a function of the activation voltage (see Figure 4C, D), one sees that the distributions are essentially identical! The Boltzmann distributions of the collisionally excited ions are expected to be broad, but as the ions exit the activation region, they are quickly thermalized due to collisions with the background He gas (3 Torr He). As the re-thermalized ion populations display the same distribution of structures, independent of the activation energy for CID, this implies a complete equilibration of structures prior to cooling.

Collisional Activation of Mobility-Selected Ions

The mobility-selected $\mathbf{a_4}$ ions at the end of the second drift tube were subjected to activation (220 V) prior to injection into the third drift tube (activations 1–3; see Figure S4). Although some $\mathbf{a_4}$ ions dissociated to smaller CID products, a considerable proportion remained as unfragmented $\mathbf{a_4}$ ions. It is then interesting to see what happens to the mobilities of the selected $\mathbf{a_4}$ ions as a result of the activation. This is shown for the three selections in Figure 5A1–3.[34] Of these selections only selection 3 can be considered a clean isolation, where no other ions are present in the selected ion population. Note that mass isolations are not possible on this instrument, and as some fragment ions have partially overlapping drift times (notably $\mathbf{a_4}$, $\mathbf{b_4}$ and $\mathbf{y_4}$; see Figure S2) this limits their complete isolation. Upon activation, the vast majority (*i.e.*, 90%) of the extended linear imine (isolation 3) is converted to higher-mobility structures, whose cross-sections are compatible with features I and II. In fact, the remaining ratio of III (10%), compared to I and II, after selection and activation is very similar to the ratio of III after CID of the precursor ion (8%). For the two other selections, similar trends are seen, although one needs to be cautious due to the interference from CID of $\mathbf{b_4}$. For selection 1, the activation results in the re-appearance of structures with reduced mobility, whose cross-sections match those of feature II. For selection 2, a substantial re-appearance of higher-mobility structures occurs, but also some appearance of lower-mobility

NIH-PA Author Manuscript

NIH-PA Author Manuscript

NIH-PA Author Manuscript

ions, which suggests a re-appearance of features I and III. All of these results are compatible with the picture that the individual structures can interconvert freely upon activation. Some readers will notice the similarity of the above approach to spectroscopic methods in supersonic expansions, where particular conformers are selected and activated, causing them to isomerize to other conformers.[35]

Activation of the mobility-3-selected ions yielded the CID mass spectrum shown in Figure 5B. Some of the subsequent CID products are expected from the linear $\mathbf{a_4}$ sequence, whereas others are more ambiguous to interpret (indicated by their masses), as they could be assigned to either direct or nondirect sequence ions.

The observed mobility shifts upon activation of linear $\mathbf{a_4}$ can be rationalized by interconversion of the linear, cyclic and unassigned structures. This suggests a complete isomerization and equilibration of the structures prior to dissociation, which is comparable to the conclusions from a previous CID study on mobility-selected ubiquitin conformers.[36]

Potential Energy Diagram

To summarize our findings, a semiquantitative potential energy surface for $\mathbf{a_4}$ is shown in Figure 6. The barriers to interconversion between different types of structures of $\mathbf{a_4}$, linear imine, cyclic and unassigned $\mathbf{a_4}$, are lower in energy than dissociation to subsequent fragments. Note that the transition state structures and energies for YGGFL $\mathbf{a_4}$ interconversions are not known; however, those for $\mathbf{a_5}$ of YAGFL-NH_2 have been calculated in detail.[2,37] In those calculations the height of the barrier for imine to cyclic conversion was found to be 13.1 kcal mol^{-1}. In Figure 6, it is assumed that the energetics for YGGFL are similar for those of YAGFL-NH_2.

Summary and Conclusions

The ion mobility results for Leu-enkephalin and its CID fragments corroborate an earlier IR spectroscopy study[20] that suggested a mixture of linear and cyclic $\mathbf{b_4}$ and $\mathbf{a_4}$ structures are formed. Here, the relative contributions of linear and cyclic structures could be approximated for $\mathbf{a_4}$, suggesting that 31% adopt a cyclic structure, whereas 8% adopt an extended linear imine structure. The remaining 61% (feature II) have cross-sections that could be rationalized with cis imine structures, although the calculated energies of these structures appear to be too high to account for their predominance in the spectrum. In the case of $\mathbf{b_4}$ the calculated cross-sections for the cyclic structures are more consistent with the experimentally determined mobility, even if the cross-sections of higher-energy oxazolone structures did approach those of cyclic structures. As oxazolone structures were confirmed in previous IR spectroscopy measurements, this strongly suggests that zero-energy structures underestimate the mobilities of room-temperature linear ions. In terms of feature II for $\mathbf{a_4}$ it is probable that other, yet unidentified, structures account for its large share of the ion population. It is clear from this and other studies that the dissociation chemistry of peptides is highly complex and that many reaction pathways have to be considered, and only some of those were considered here.

These results also underline the importance of validating some of the ion mobility results with other structural techniques, such as isotope labeling[38] and IR spectroscopy. In the case of peptide CID fragment ions the chemical information available from IR spectroscopy would be highly complementary and may confirm the structural identity of, *e.g.*, feature II of this study. Multiple gas-phase structural tools are necessary to address the structural complexity of peptide fragment ions, as they can differ in the chemical moieties that are formed and the site where the proton is attached. Moreover, the appearance of mixtures of

NIH-PA Author Manuscript

NIH-PA Author Manuscript

NIH-PA Author Manuscript

fragment ions is likely not be limited to Leu-enkephalin, as others have observed multiple structures for particular CID product ions by ion mobility.[22,28]

Finally, this study showed that the relative abundances of $\mathbf{a_4}$ structures formed in CID are independent of the total energy deposited in the molecule, though this clearly does affect the individual fragment ion abundances in the CID mass spectrum. Moreover, extensive isomerization of $\mathbf{a_4}$ structures takes place during activation, thereby apparently preventing structure-dependent CID. In other words, the molecules lose all memory of the conformation that they had prior to collisional activation, which could cause scrambling of the primary structure of the peptide to occur independent of the starting structure of the peptide.

Supplementary Material

Refer to Web version on PubMed Central for supplementary material.

Acknowledgments

We gratefully acknowledge support from the NIH (NIH#R01-AG-024547) and NSF (NSF#CHE-0078737) that allowed for development of instrumentation used in this study. N.P. thanks the University of Florida for providing generous start-up funds. B.P. acknowledges the DFG for their support (SU 244/3-1).

References and Notes

1. Vachet RW, Bishop BM, Erickson BW, Glish GL. J Am Chem Soc. 1997; 119:5481–5488.
2. Harrison AG, Young AB, Bleiholder C, Suhai S, Paizs B. J Am Chem Soc. 2006; 128:10364–10365. [PubMed: 16895391]
3. Biemann K, Scoble HA. Science. 1987; 237:992–998. [PubMed: 3303336]
4. Chait BT, Wang R, Beavis RC, Kent SBH. Science. 1993; 262:89–92. [PubMed: 8211132]
5. Abersold R, Goodlett DR. Chem ReV. 2001; 101:269–295. [PubMed: 11712248]
6. Steen H, Mann M. Nature ReV Mol Cell Biol. 2004; 5:699–711. [PubMed: 15340378]
7. Eng JK, McCormack AL, Yates JR III. J Am Soc Mass Spectrom. 1994; 5:976–989.
8. Perkins DN, Pappin DJC, Creasy DM, Cottrell JS. Electrophoresis. 1999; 20:3551–3567. [PubMed: 10612281]
9. Simpson RJ, Connolly LM, Eddes JS, Pereira JJ, Moritz RL, Reid GE. Electrophoresis. 2000; 21:1707–1732. [PubMed: 10870958]
10. Paizs B, Suhai S. Mass Spectrom ReV. 2005; 24:508–548. [PubMed: 15389847]
11. Roepstorff P, Fohlmann J. Biomed Mass Spectrom. 1984; 11:601. [PubMed: 6525415]
12. Dongré AR, Jones JL, Somogyi A, Wysocki VH. J Am Chem Soc. 1996; 118:8365–8374.
13. Wysocki VH, Tsaprailis G, Smith LL, Breci LA. J Mass Spectrom. 2000; 35:1399–1406. [PubMed: 11180630]
14. Biemann K. Biomed EnViron Mass Spectrom. 1988; 16:99–111. [PubMed: 3072035]
15. Cordero MM, Houser JJ, Wesdemiotis C. Anal Chem. 1993; 65:1594–1601. [PubMed: 8328675]
16. Yalcin T, Khouw C, Csizmadia IG, Peterson MR, Harrison AG. J Am Soc Mass Spectrom. 1995; 6:1165–1174.
17. Yalcin T, Csizmadia IG, Peterson MR, Harrison AG. J Am Soc Mass Spectrom. 1996; 7:233–242.
18. Paizs B, Szlávik Lendvay G, Vekey K, Suhai S. Rapid Commun Mass Spectrom. 1999; 13:525–533.
19. Polfer NC, Oomens J, Suhai S, Paizs B. J Am Chem Soc. 2005; 127:17154–17155. [PubMed: 16332041]
20. Polfer NC, Oomens J, Suhai S, Paizs B. J Am Chem Soc. 2007; 129:5887–5897. [PubMed: 17428052]

NIH-PA Author Manuscript

NIH-PA Author Manuscript

NIH-PA Author Manuscript

21. (a) Herrmann KA, Kuppannan K, Wysocki VH. Int J Mass Spectrom. 2006; 249:93–105. [PubMed: 18802500] (b) Galhena A, Somogyi A, Perkins B, Wysocki VH. Proc Conf Am Soc Mass Spectrom. 2007; 55
22. Riba I, Giles K, Gaskell SJ. Proc Conf Am Soc Mass Spectrom. 2007; 55
23. Clemmer DE, Jarrold MF. J Mass Spectrom. 1997; 32:577–592.
24. Wyttenbach T, Bowers MT. Top Curr Chem. 2003; 225:207–232.
25. Fenn JB, Mann M, Meng CK, Wong SF, Whitehouse CM. Science. 1989; 246:64–71. [PubMed: 2675315]
26. Merenbloom SI, Koeniger SL, Valentine SJ, Plasencia MD, Clemmer DE. Anal Chem. 2006; 78:2802–2809. [PubMed: 16615796]
27. Tang K, Shvartsburg AA, Lee HN, Prior DC, Buschbach MA, Li FM, Tolmachev AV, Anderson GA, Smith RD. Anal Chem. 2005; 77:3330–3339. [PubMed: 15889926]
28. Koeniger SL, Merenbloom SI, Valentine SJ, Jarrold MF, Udseth HR, Smith RD, Clemmer DE. Anal Chem. 2006; 78:4161–4174. [PubMed: 16771547]
29. Koeniger SL, Merenbloom SI, Sevugarajan S, Clemmer DE. J Am Chem Soc. 2006; 128:11713–11719. [PubMed: 16939296]
30. Counterman AE, Valentine SJ, Srebalus CA, Henderson SC, Hoaglund CS, Clemmer DE. J Am Soc Mass Spectrom. 1998; 9:743–759. [PubMed: 9692251]
31. Thalassinos K, Hoyes J, Slade SE, Jennings KR, Scrivens JH, Giles K, Wildgoose J, Hoyes J, Bateman RH, Bowers MT. Int J Mass Spectrom. 2004; 236:55–63.
32. Mesleh MF, Hunter JM, Shvartsburg AA, Schatz GC, Jarrold MF. J Phys Chem. 1996; 100:16082–16086.
33. Schnier PD, Price WD, Strittmatter EF, Williams ER. J Am Soc Mass Spectrom. 1997; 8:771–780. [PubMed: 16554908]
34. To convert the drift time distributions in Figure S4 to cross-section distributions in Figure 5 A1–3, one should note that the shift in mobility as a result of activation only affects the drift time in the third drift tube. Conversely, the mobility-selected a_4 ions, originally generated from precursor Leu-enkephalin, were separated over the length of two drift tubes. It is clear that the separation in drift time over 1 drift tube is merely half of the separation over two drift tubes. This has been taken into account to determine the cross-section distributions in Figure 5. Moreover, the decrease in drift time due to the activation voltage has been corrected for in the cross-section distributions.
35. Zwier TS. J Phys Chem A. 2006; 110:4133–4150. [PubMed: 16553364]
36. Badman ER, Hoaglund-Hyzer CS, Clemmer DE. J Am Soc Mass Spectrom. 2002; 13:719–723. [PubMed: 12056571]
37. Bleiholder C, Cooper T, Groves J, Young AB, Suhai S, Van Stipdonk M, Harrison AG, Paizs B. Manuscript in preparation.
38. Cooper T, Talaty E, Grove J, Van Stipdonk M, Suhai S, Paizs B. J Am Soc Mass Spectrom. 2006; 17:1654–1664. [PubMed: 16934997]

NIH-PA Author Manuscript

NIH-PA Author Manuscript

NIH-PA Author Manuscript

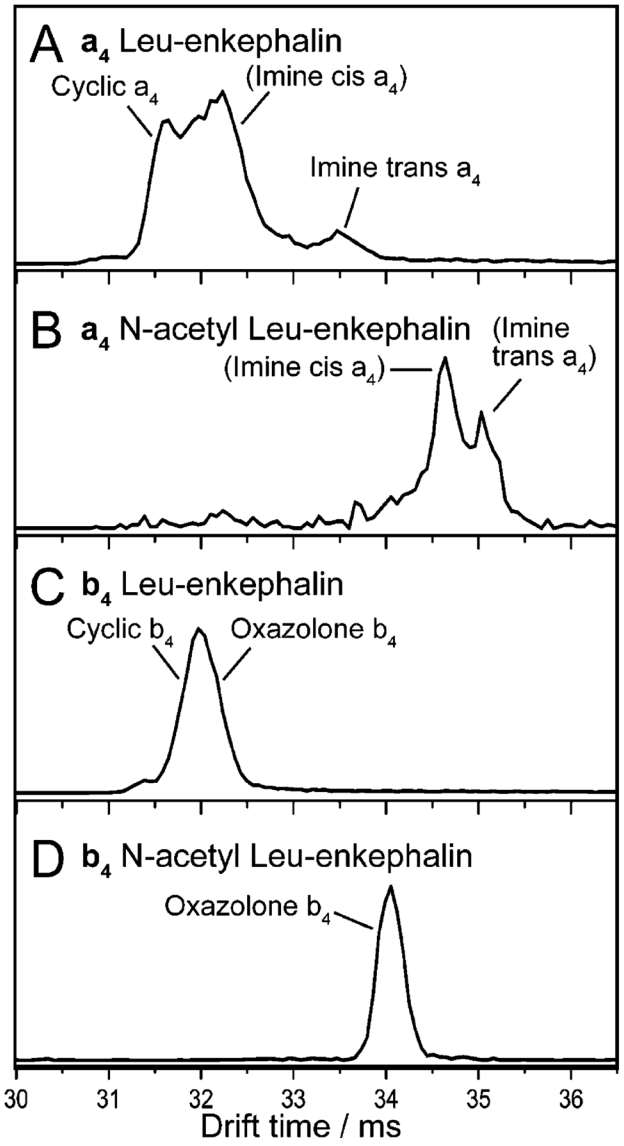

Figure 1.

Drift time distributions for the CID product ions (A) a_4 of Leu-enkephalin, (B) a_4 of *N*-acetyl Leu-enkephalin, (C) b_4 of Leu-enkephalin, and (D) b_4 of *N*-acetyl Leu-enkephalin (activation voltage 230 V). The structural assignments of the mobility-separated peaks are tentatively indicated and can only be confirmed theoretically in some cases; the more hypothetical assignments have been indicated by brackets. Note that these drift time distributions have been determined for the length of the whole instrument (*i.e.*, 2.9 m).

NIH-PA Author Manuscript
NIH-PA Author Manuscript
NIH-PA Author Manuscript

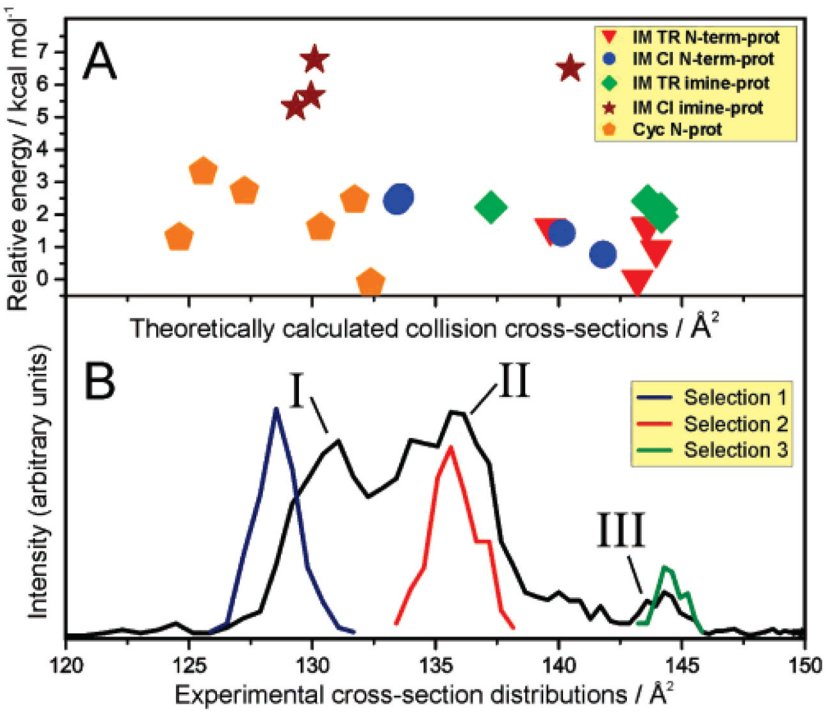

Figure 2.

(A) Theoretical cross-sections and relative energies for the density-functional theory calculated structures of the lowest-energy imine and cyclic variants of a_4 for Leu-enkephalin. The legend indicates the different imine variants, showing the cis and trans isomers and the site of proton attachment. (B) Experimentally determined cross-section distribution of a_4, based on the mobilities through the second drift tube. Mobility selections (1–3) were also carried out at the end of the second drift tube, as explained in the Methods. Note that the intensities of the mobility selections are increased by a factor of 40 relative to the unselected a_4 distribution. The three distinct features in the mobility spectrum are labeled as I, II and III.

NIH-PA Author Manuscript
NIH-PA Author Manuscript
NIH-PA Author Manuscript

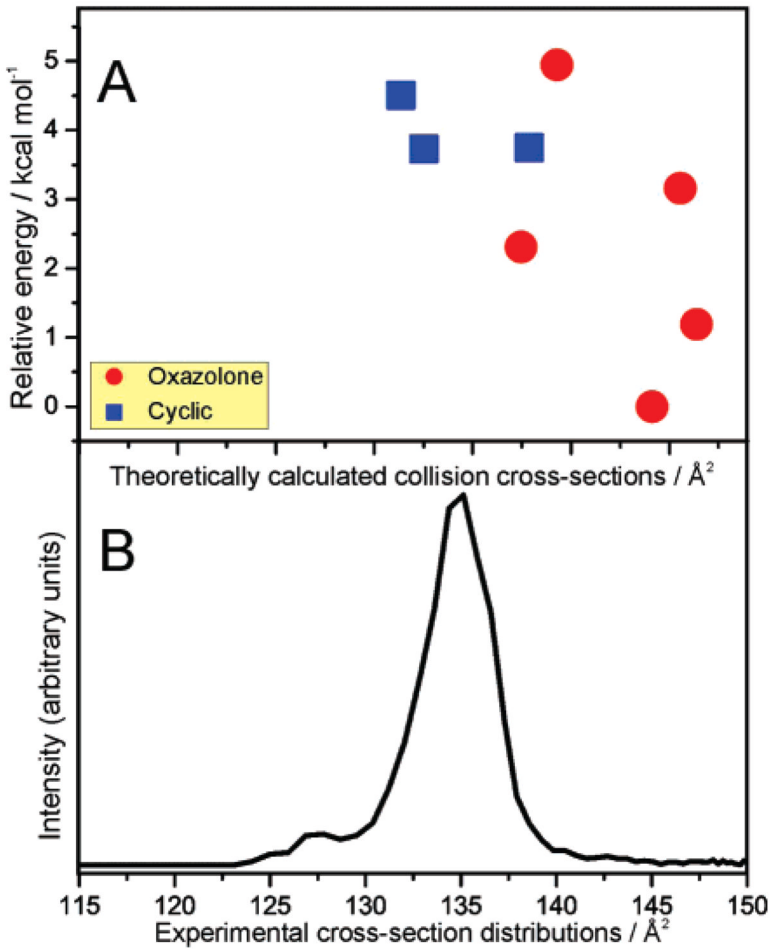

Figure 3.
(A) Theoretical cross-sections and relative energies for the density-functional theory calculated structures of the lowest-energy oxazolone (red circles) and cyclic (blue squares) isomers for Leu-enkephalin b_4. (B) Experimental cross-section distributions for b_4.

NIH-PA Author Manuscript

NIH-PA Author Manuscript

NIH-PA Author Manuscript

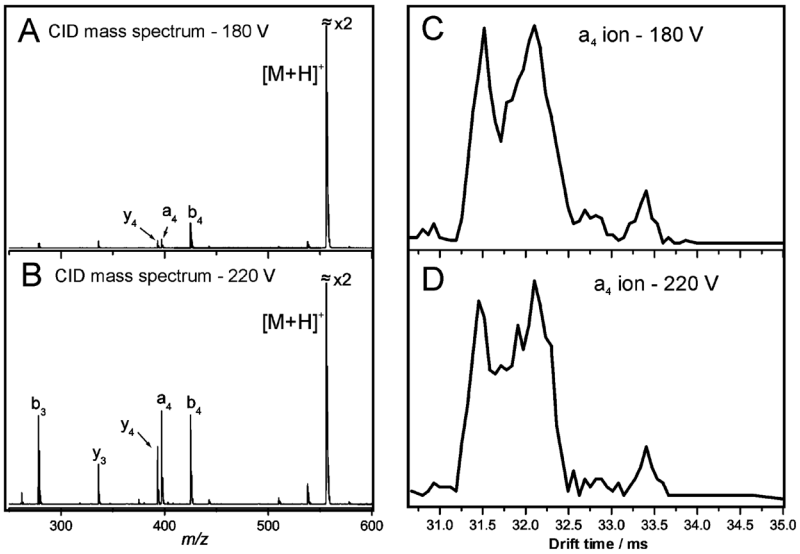

Figure 4.

CID mass spectra of singly protonated Leu-enkephalin $[M+H]^+$ for activation energies of (A) 180 V and (B) 220 V. Note that the vertical intensity scale is expanded by a factor of 2. Total drift time distributions of the a_4 fragment ion for activation energies of (C) 180 V and (D) 220 V.

NIH-PA Author Manuscript
NIH-PA Author Manuscript
NIH-PA Author Manuscript

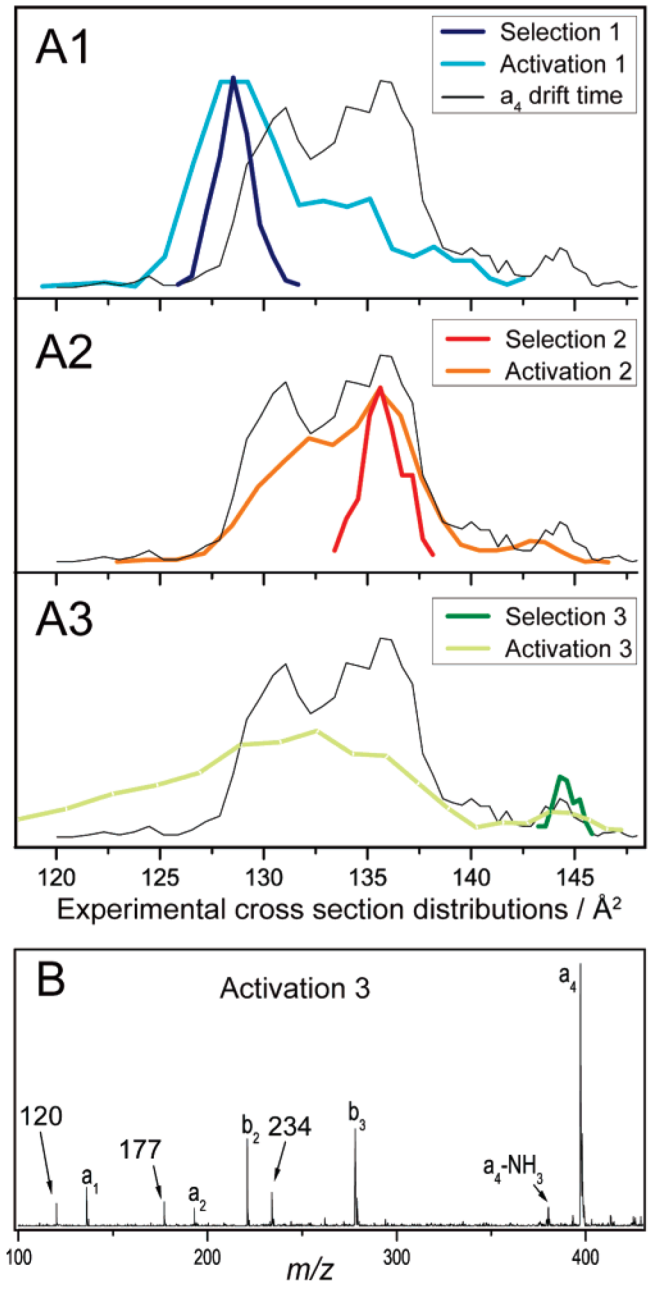

Figure 5.

(A1–3) Cross-section distributions of mobility-selected ions prior to and after collisional activation. The drift time distribution of the whole a_4 distribution is indicated with a fine line as a reference. Note that the intensity scale has been arbitrarily normalized to allow for a better comparison. (B) CID mass spectrum of mobility-selected a_4, using mobility selection 3 from above. The expected **a** and **b** ions are indicated, as well as the masses of other fragment ions that are less straightforward to interpret.

NIH-PA Author Manuscript

NIH-PA Author Manuscript

NIH-PA Author Manuscript

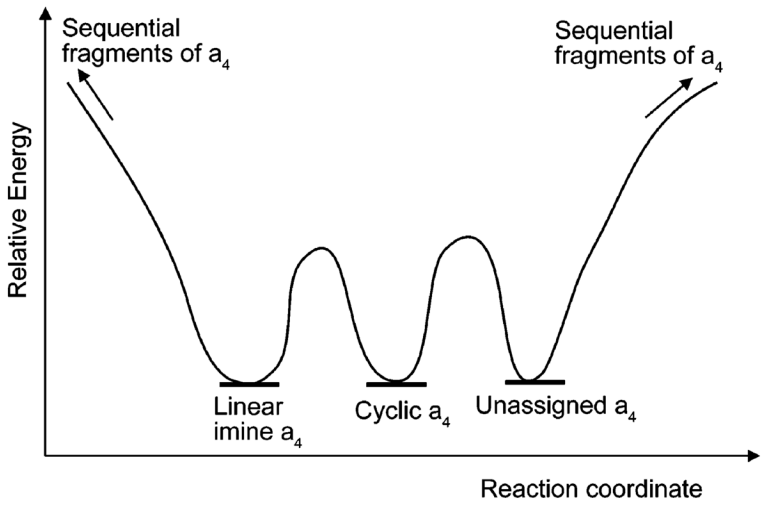

Figure 6.

Semiquantitative potential energy diagram for the reaction pathway for CID of linear a_4. In this simplified diagram the relative energies for each chemical structure are shown as a function of the reaction coordinate, as well as the transition state energies for interconversion. The linear imine and cyclic structures are almost isoenergetic. The energy of the unassigned structure is not known but cannot be higher than either the linear or cyclic structures, given its high abundance. The height of the transition states are lower in energy than the sequential dissociation to smaller CID products.

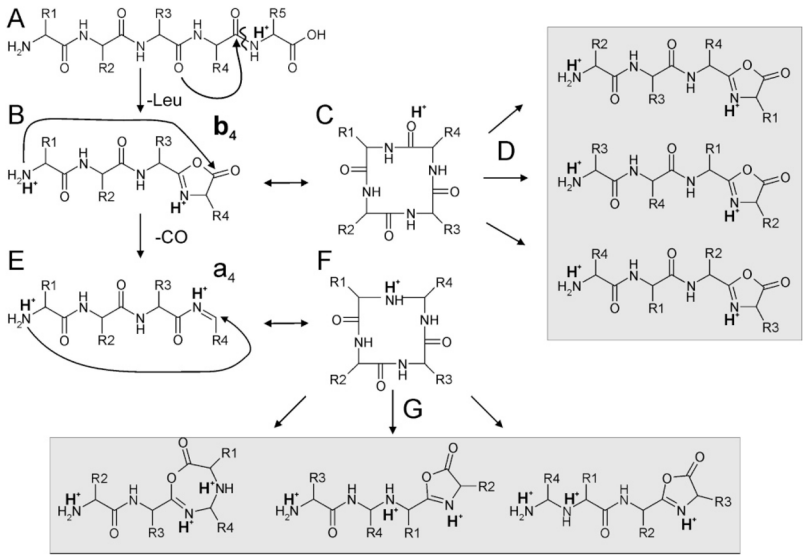

SCHEME 1. Reaction Scheme for Generating b_4 and a_4 CID Product Ions from the Protonated Leu-Enkephalin Pentapeptide Precursor Ion[a]

[a] Note that the side chains are denoted as R1 = CH_2–C_6H_4–OH, R2 = R3 = H and R4 = CH_2–C_6H_5. (A) The reactive configuration of the precursor ion allows a nucleophilic attack of the carbonyl oxygen of residue 3 on the carbonyl carbon of residue 4. This results in the cleavage of the amide bond between residues 4 and 5, leading to b_4 and neutral Leu products. (B) The resulting b_4 is thought to have a five-membered "oxazolone" ring. Note that the proton is exclusively retained by the N-terminal fragment, by virtue of its higher proton affinity compared to Leu. (C) This structure can isomerize to a fully cyclic structure following nucleophilic attack from the N-terminus. A re-opening of the ring can lead to the original oxazolone structure in B or alternatively lead to linear oxazolone structures (D), which do not reflect the original amino acid sequence (gray box). (E) Sequential loss of CO from b_4 results in a_4, which is thought to have a linear imine structure. Note that cis and trans imine isomers have to be considered here. (F) In analogy to b_4 this structure can isomerize to a cyclic structure, which can open up at amide bonds on b_n-y_m-like PFP's, once again resulting in (G) oxazolone-type structures with permutated amino acid sequences (gray box). Alternatively, the cyclic structure can revert back to the original linear imine structure. Note that subsequent CID of the structures with permutated sequences rationalizes the appearance of "nondirect" sequence ions, which cannot be explained on the basis of the original amino acid sequence. Note also that the most probable sites of proton attachment for each fragment structure are indicated, multiple sites being possible for the linear b_4 and a_4 fragments.

NIH-PA Author Manuscript NIH-PA Author Manuscript NIH-PA Author Manuscript

NIH-PA Author Manuscript

NIH-PA Author Manuscript

NIH-PA Author Manuscript

TABLE 1

Theoretical Collision Cross-Sections ($Å^2$) and Standard Deviations for the Structural Variants of Leu-Enkephalin a_4, Shown in Figure 2A, and b_4, Shown in Figure 3A

structural variants of a_4	**calculated collision cross-section/$Å^2$**
imine trans N-term	143 ± 2
imine cis N-term	137 ± 4
imine trans imine N	142 ± 3
imine cis imine N	132 ± 5
cyclic	129 ± 3
structural variants of b_4	calculated collision cross-section/$Å^2$
oxazolone	142 ± 4
cyclic	132 ± 3